

Article

A Novel Parametric Modeling Method and Optimal Design for Savonius Wind Turbines

Baoshou Zhang ^{1,*}, Baowei Song ¹, Zhaoyong Mao ¹, Wenlong Tian ¹, Boyang Li ^{2,3} and Bo Li ¹

¹ School of Marine Science and Technology, Northwestern Polytechnical University, Xi'an 710072, Shaanxi, China; songbaowei@nwpu.edu.cn (B.S.); maozhaoyong@nwpu.edu.cn (Z.M.); tianwenlong@mail.nwpu.edu.cn (W.T.); boli121@sina.com (B.L.)

² College of Electromechanical Engineering, Qingdao University of Science and Technology, Qingdao 266061, Shandong, China; qdlby@126.com

³ Marine Engineering Department, Qingdao Ocean Shipping Mariners College, Qingdao 266071, Shandong, China

* Correspondence: zbsnwpu@sina.com; Tel.: +86-187-9254-7553

Academic Editor: Frede Blaabjerg

Received: 27 November 2016; Accepted: 28 February 2017; Published: 3 March 2017

Abstract: Under the inspiration of polar coordinates, a novel parametric modeling and optimization method for Savonius wind turbines was proposed to obtain the highest power output, in which a quadratic polynomial curve was bent to describe a blade. Only two design parameters are needed for the shape-complicated blade. Therefore, this novel method reduces sampling scale. A series of transient simulations was run to get the optimal performance coefficient (power coefficient C_p) for different modified turbines based on computational fluid dynamics (CFD) method. Then, a global response surface model and a more precise local response surface model were created according to Kriging Method. These models defined the relationship between optimization objective C_p and design parameters. Particle swarm optimization (PSO) algorithm was applied to find the optimal design based on these response surface models. Finally, the optimal Savonius blade shaped like a “hook” was obtained. C_m (torque coefficient), C_p and flow structure were compared for the optimal design and the classical design. The results demonstrate that the optimal Savonius turbine has excellent comprehensive performance. The power coefficient C_p is significantly increased from 0.247 to 0.262 (6% higher). The weight of the optimal blade is reduced by 17.9%.

Keywords: Savonius wind turbine; parametric model; polar coordinates; computational fluid dynamics (CFD); Kriging method; particle swarm optimization (PSO)

1. Introduction

In recent years, the gradually exhausting non-renewable energy resources and economic viability stimulate the development of renewable energy technology. The use of Savonius wind turbines is within of this context, but Savonius wind turbines are still not widespread. Savonius turbines are suitable for many scenarios, such as the small and medium-sized distributed power generation [1]. Main advantages of Savonius wind turbines can be described as follows: high starting up and full operation moment; operate in a wide range of wind conditions; simple construction with low cost; low noise emission and stable performance [2–4]. Altan et al. [5] and Tian et al. [2] have explained the work principle of a Savonius rotor by analyzing the main flows around the turbine.

However, relatively low efficiency of Savonius turbines is a great limitation. Therefore, different efforts are directed towards finding a better design for Savonius turbines, which will improve its performance. Some previous studies have suggested many different modified methods to obtain the optimal Savonius turbine. The “optimal” means that the Savonius wind turbine has its highest

power coefficient C_p (optimization objective). The performance of Savonius turbines is affected by the blade geometry, blade spacing and overlap, blades number, end plates, turbines stages, guide plates and other accessories [3,4]. Wahyudi et al and Kumar et al. [6,7] used obstacle plates or deflectors to optimize the design of Savonius blade turbine. Classical and improved Savonius wind turbines have been studied by Kacprzak et al. [8]. The slot position, which affects the starting torque for a Savonius wind turbine, was analyzed by Alaimo et al. [9]. Altanet al. proposed that a wind deflector with a simple construction could be designed to enhance the performance of the Savonius wind rotor [10]. Similarly, El-Askary et al. [11] added a series of guide plates to harvest the incoming wind.

The above studies focus on using a segment of circular arc as a Savonius turbine blade. It is clear that the blade geometry or shape is the basis of the optimal design for other design variables, such as obstacle plates and guide plates, etc. However, there are still few studies about the blade geometry. Modi et al. study the blade geometry and aspect ratio, by an extensive wind-tunnel test program [12]. The Bach-type Savonius is studied by Tong et al to obtained better performance [13]. Mohamed et al. [14] considered six free parameters in an optimization process to increase the efficiency of the Savonius turbine. Finally, they got a flat shape blade. However, most of the optimizations for the Savonius turbine had become very overcomplicated. Driss et al. [15] used 12 parameters to define a Savonius turbine and got a segment of circular arc as the blade (arc angle $\psi = 120^\circ$). Ahmed et al. suggested the optimum blade curvature for maximum energy extraction was found to be 70° (blade arc angle) [16]. Al-Faruk et al. studied the blade arc angle and the higher aspect ratio at the same time [17]. The performance comparison of optimum configuration with conventional Savonius rotor showed an increase of 24.12%. Al-Faruk et al. suggested power coefficients increase with the increase of blade arc angle up to a certain optimal value of 195° . Kacprzak et al. [8] suggested the optimum blade was composed of a segment of circular arc and a short straight line segment. However, this optimum blade was still built based on a segment of circular arc.

In this paper, we work on depicting a shape-complicated blade with minimal design parameters. A pure parametric model for the blade (that is not a kind of circular arc) is presented, and only the shape of blade is investigated in the optimization process. Under the inspiration of polar coordinates, a second order polynomial is bent to describe a blade. In mathematics, the polar coordinate system determines a point by a distance and an angle. This is similar to describing the shape of the turbine blade. This parametric modeling method can simplify design parameters and improve the efficiency of the optimization model. It also suggests that higher order curve could be used to describe a more precise blade in the future. According to the design parameters, new blades could be built. The performance of Savonius turbines is investigated using computational fluid dynamics (CFD) method. The effectiveness of CFD methods is proved by similar research conducted in similar studies [3,18].

How to build surrogate model for the optimization process is a key element. Kriging Method proposed by Danie G. Krige in 1951 is used as a surrogate model to build response surfaces. Kriging Method is an unbiased estimation model with minimum variance. The relationship (response surface model) between optimization objective C_p and design parameters could be precisely defined according to Kriging model [19]. Then, a highly effective optimization method must be selected to solve the Kriging model. Inspired by observing the natural swarming behavior of bird flocking, particle swarm optimization (PSO) was raised [20,21]. PSO algorithm is simple in concept, easy to implement and computationally inexpensive [22]. Accordingly, the PSO algorithm was modified and used to find the optimal design parameters for the blade based on the response surfaces built by Kriging method.

Through a series of iterations, the optimal shape of the Savonius blade was built to obtain its highest power coefficient C_p , which is the crucial first step of the overall optimization considering other design variables. Moreover, it will enrich the parametric modeling method and optimization ideology for future Savonius turbines studies.

2. Geometry Configuration

2.1. Parametric Modeling Method

A novel parametric modeling method was presented. It is an inspiration from polar coordinates. Polar coordinate system is a 2D coordinate system in which each point on a plane is determined by a distance from a reference point and an angle from a reference direction. The reference point (analogous to the origin of a Cartesian system) is called the pole, and the ray from the pole in the reference direction is the polar axis. The distance from the pole is called the polar radius, and the angle is called the polar angle. First of all, a quadratic polynomial curve defined by Equation (1) was drawn, as shown in Figure 1a. $y = 0.025x^2 - 0.07x + 0.1884$ is regarded as an example. Analogous to the polar coordinate system, the value of horizontal axis x was set to polar angle, spanning approximately from $-\pi/2$ rad to $+\pi/2$ rad. The value of vertical axis y was set to polar radius. Finally, the polar radius was rotated along with the polar angle changing from $-\pi/2$ rad to $+\pi/2$ rad. It means that the curve is bent and rotated to generate a more precise blade. The profile shape of the blade was drawn, as shown in Figure 1b. Two origin-symmetric blades rotate around the central axis and make a Savonius turbine rotor.

$$y = a_2x^2 + a_1x + a_0 \tag{1}$$

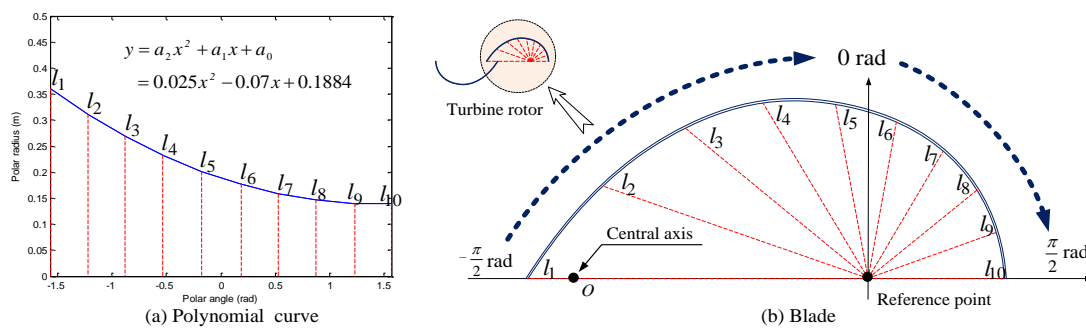


Figure 1. Polynomial curve and the corresponding blade.

The configuration of classical Savonius turbine was defined based on numerical simulation model presented in a similar literature [2] and wind tunnel model presented in a study from US Sandia Laboratories [23]. The Savonius turbine is shown in Figure 2. Simplified 2D model can be used to describe Savonius turbine rotors, as shown in Figure 2b,c. D represents the rotor diameter; H represents the rotor height; d represents the length of blade; h represents the height of blade; r represents the radius of the classical blade (semicircle blade); and S_0 represents the length of two blades overlap. Undisturbed velocity of a wind is v_∞ . These turbine rotors are submitted to the wind with rotation rate ω .

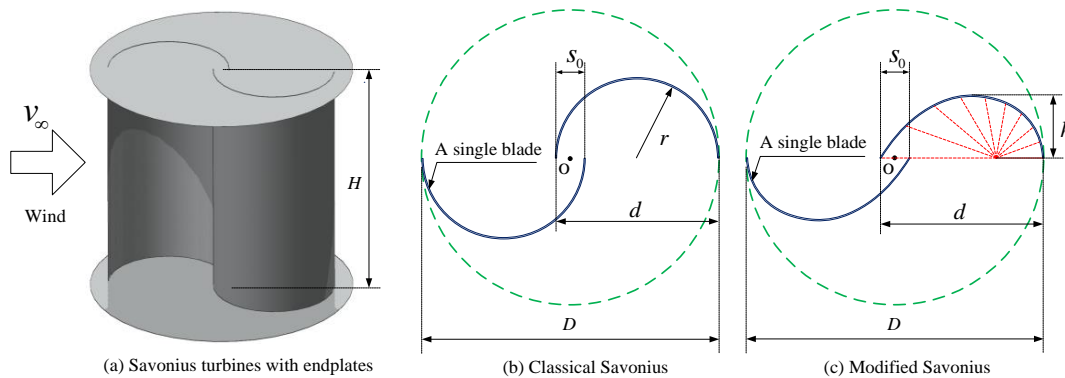


Figure 2. (a) Savonius wind turbines; and (b,c) simplified 2D model.

In this study, the blade shape will be optimized. Thus, the effect of other variables should be removed. Hence, the overall size of the modified Savonius is set equal to the classical Savonius. The parameters such as $D, H, d,$ and S_0 are same [24,25]. To guarantee the consistency of the overall shape, a main constraint condition, that the length of a blade d is the same, is shown as follows:

$$\begin{cases} d = y_{-\pi/2} + y_{+\pi/2} & \text{(Modified Savonius)} \\ d = 2r & \text{(Classical Savonius)} \end{cases} \quad (2)$$

Equation (2) can be further transformed into:

$$d = a_2(-\pi/2)^2 + a_1(-\pi/2) + a_0 + a_2(\pi/2)^2 + a_1(\pi/2) + a_0 = 2r \quad (3)$$

$$a_0 = r - (\pi/2)^2 a_2 \quad (4)$$

In this process, a_0 can be expressed by a_2 . By removing unconcerned variables, the number of design parameters is further reduced. Main geometrical parameters of the classical Savonius turbine and the modified Savonius turbine are listed in Table 1.

Table 1. Main geometrical parameters of turbine rotors.

Type of the Turbines	D (m)	H (m)	d (m)	S_0 (m)	r (m)	h
Classical Savonius	0.909	1.0	0.5	0.091	0.25	0.25
Modified Savonius	0.909	1.0	0.5	0.091	$y_{a_2 a_1}(x)$	–

Because $r = 0.25$, Equation (4) is expressed as $a_0 = 0.25 - (\pi/2)^2 a_2$. Equation (1) is transformed into:

$$y = a_2 x^2 + a_1 x + 0.25 - (\pi/2)^2 a_2 \quad (5)$$

Thus, a_2 and a_1 define the corresponding quadratic polynomial curve. Meanwhile, the blade of the modified Savonius turbine rotor needs to meet two assumptions: (1) the blade is convex; and (2) h is the length and ranges between 0 and 2 times of r . Thus, the blade shape is limited in the normal range by these assumptions. Accordingly, a_2 and a_1 could not be selected at random. The selection space that satisfies all the constraints and assumptions is called feasible region. Feasible region of a_2 and a_1 is precisely defined, as shown in Figure 3. Nine typical sample points are selected in the feasible region as examples. According to the nine sample points $P_N(a_2, a_1)$, the corresponding blades are drawn, as shown in Figure 3.

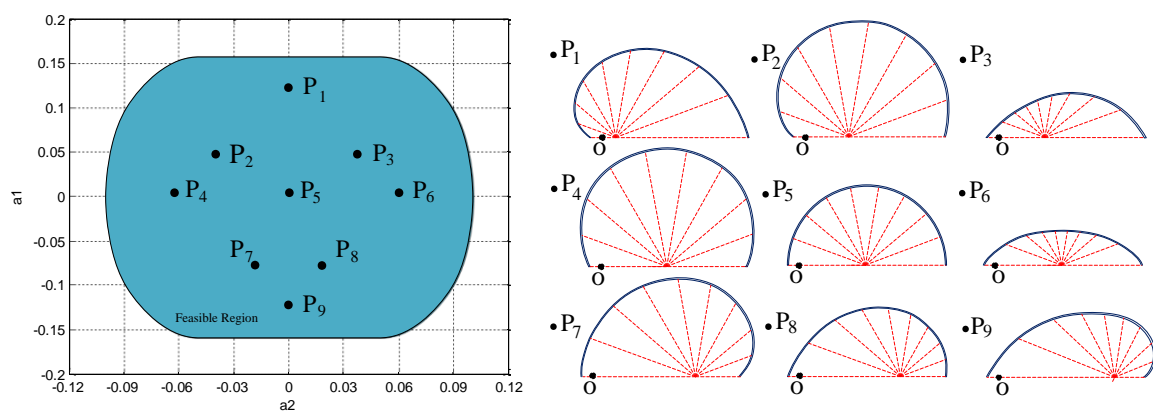


Figure 3. Feasible region (a_2 and a_1), nine typical points and blades.

A series of shape-complicated blades can be described using only two design parameters. Corresponding nine groups of design parameters (sample points) are listed in Table 2.

Table 2. Nine groups of design parameters.

Design Parameters	a_2	a_1	Design Parameters	a_2	a_1
P_1	0	0.12	P_6	0.06	0
P_2	−0.05	0.04	P_7	−0.02	−0.08
P_3	0.05	0.04	P_8	0.02	−0.08
P_4	−0.06	0	P_9	0	−0.12
P_5	0	0	–	–	–

2.2. Coefficient of Performance

Tip speed ratio (*TSR*) means the ratio between rotor blade tip speed and inflow air speed and is defined as follows:

$$TSR = \omega D / (2v_\infty) \quad (6)$$

Two indicators are used to describe the performance of Savonius wind turbines: torque coefficient (C_m) and power coefficient (C_p). C_p represents the fraction of extracted power from the total power of air flow which runs through the projected area of turbines at the flow direction. Power coefficient C_p is mainly used to evaluate the comprehensive performance of Savonius turbines. Therefore, the optimization objective is C_p . C_m and C_p can be obtained as follows:

$$C_m = 4M / (\rho H v_\infty^2 D^2) \quad (7)$$

$$C_p = P / (0.5 \rho H D v_\infty^3) = 2M\omega / (\rho H D v_\infty^3) = C_m \cdot TSR \quad (8)$$

where M is the torque acting on Savonius turbines; P is the power; Since only 2D simulations were performed, the unit height $H = 1$ m was used [26]. ρ is the air density.

3. Numerical Method

In the whole optimization process, numerical method using Ansys Fluent provides foundation elements for the modeling of the response surface surrogate model (established by using Kriging method). The fluid forces, moments, angular velocities, etc. acting on these turbines could be obtained separately. Therefore, the performance (power coefficient C_p) of different turbine is obtained. A series of transient, 2D representations of the flow field was built. Hence, the flow in the vertical direction was neglected, which is equivalent to 3D Savonius rotors with endplates. It was already successfully proved in similar studies using Ansys Fluent [6,8,27]. Due to the low velocity (7 m/s) in the flow [26], basic assumptions are presented:

- (1) Temperature and density variation of the flow was negligible.
- (2) The relative velocity is assumed to be vector having constant direction.
- (3) The rolling resistance of the rotor shaft is not included in the simulation.

3.1. Computational Domains and Grid Generation

Two fluid domains were created. Rotating domain and stationary domain are shown in Figure 4. The computational domain has a width of 20D and a length 30D ($D = 0.909$ m is the diameter of the rotor). The turbine was placed in the symmetry axis of the top and bottom boundary and at a distance of 10D from the left boundary. Since the computational domain is large enough, the outlet is far enough away from the rotating domain. The distance between the outlet and the rotating domain is 20 times the width of the turbine rotor. According to the practical simulation results, the pressure of outlet could remain stable. Similarly, the side walls are far enough away from the rotating domain.

The width of the computational domain is 20 times the width of the turbine rotor. The pressure of side walls remains stable. The side walls have no effect on the turbine rotor. Therefore, blockage effects could be excluded. Boundary conditions are set as follows:

- (1) Inlet: The velocity-inlet was set to be equivalent to inlet depending on the desired *TSR*.
- (2) Outlet: Relative atmospheric pressure was set to be 0 Pa.
- (3) Interface: The border between rotating domain and stationary domain was set to interface.
- (4) No slip wall: No slip wall conditions were imposed on the blades.

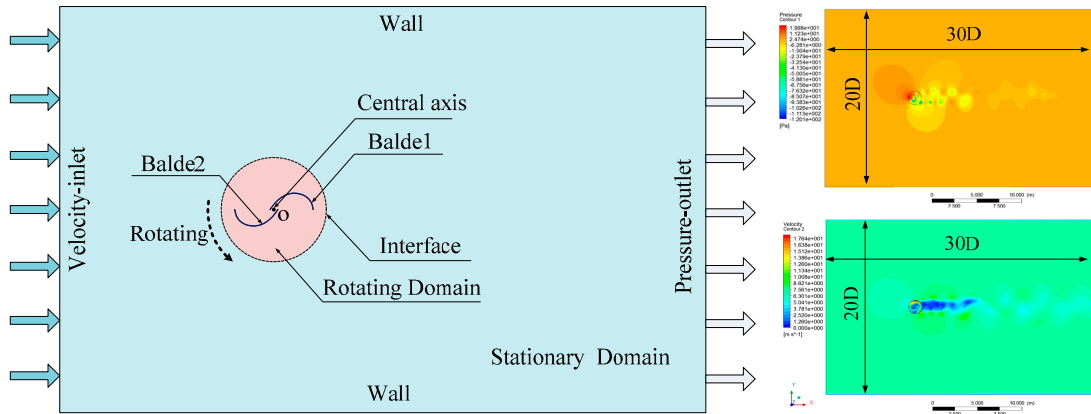


Figure 4. Simulation domains.

Savonius turbine rotor rotates around the central axis. The rotating domain moves exactly 1.0° every step. Four type relative rotation positions and local details of the mesh are shown in Figure 5. In the CFD simulations, the Finite Volume Method (one of the most versatile discretization techniques) is used. The smallest size of the mesh is smaller than 0.4 mm. There are eight prism layers, with a layer growth rate of 1.2.

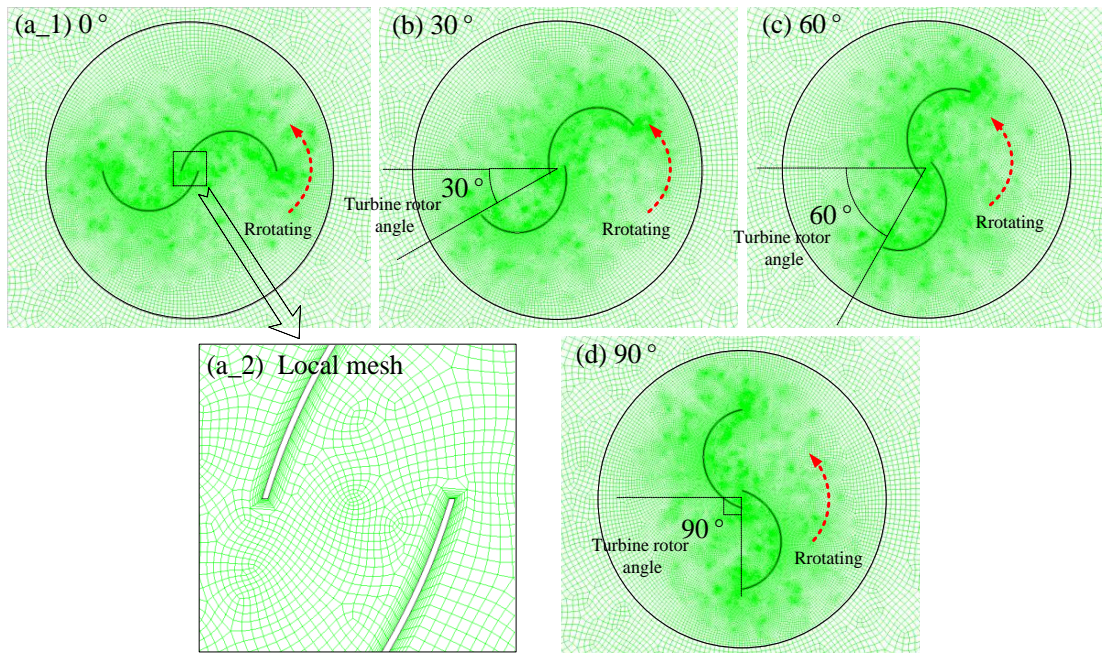


Figure 5. Relative rotation positions around the blades at different rotor angle.

3.2. Numerical Method Validation

Mesh independence validation study and a time step independent studies were conducted respectively. The verification simulations were conducted ($v = 7$ m/s, $TSR = 1.0$). Mesh independence was tested by assessing the instantaneous torque of a single blade with different mesh densities. The instantaneous C_p is presented in Figure 6a. The average C_p is listed in Table 3. The different C_p has the great consistency for different mesh (61,000/86,900/117,000 elements). Accordingly, the mesh with approximately 60,000 elements was sufficient for the mesh independent study.

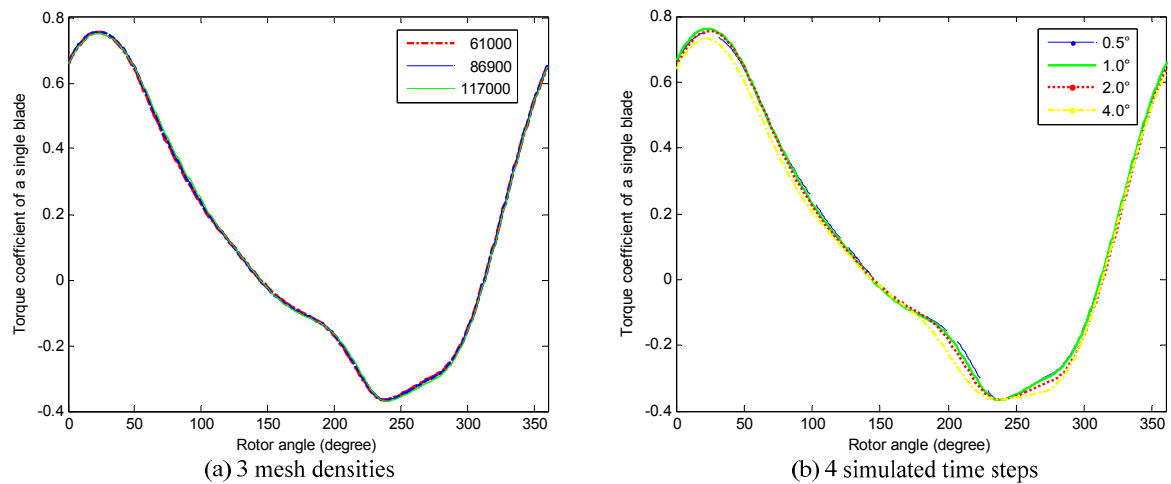


Figure 6. (a) Three mesh densities and (b) four time steps: comparison of the torque coefficient at different rotor angle.

The time step independent validation was conducted using different time steps ranging from $0.5^\circ/\text{step}$ to $4^\circ/\text{step}$. The instantaneous C_p presented in Figure 6b. The average C_p listed in Table 3 has the great consistency. Taking the simulation efficiency into consideration, $1.0^\circ/\text{step}$ was selected for subsequent studies.

Table 3. Average C_p for different densities and time steps.

Grid Number	Average C_p	Time Step	Average C_p
61,000	0.24750	0.5	0.24783
86,900	0.24871	1.0	0.24750
117,000	0.24723	2.0	0.24803
—	—	4.0	0.24610

To verify the feasibility of the numerical method, simulation data were processed to compare with wind tunnel data presented by US Sandia Laboratories [23]. The CFD domain in this section is the same as that in Section 3.1. The computational domain has a width of 20D and a length 30D. Since the computational domain is large enough, blockage effects can be excluded. Finally, simulation results are consistent well with the experiment data, although there are some subtle differences, as shown in Figure 7. Therefore, the numerical method using Fluent is acceptable.

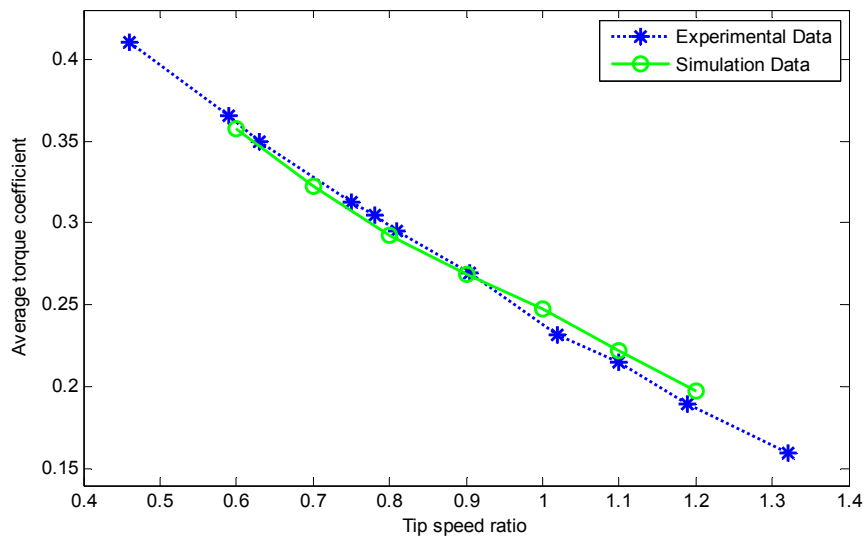


Figure 7. Comparison of the average torque coefficient at different tip speed ratios (TSRs).

3.3. Simulation Example

A blade built using design parameters $a_2 = 0.02$ and $a_1 = -0.03$ is considered in this section. In the numerical simulation process, the cyclical torque coefficient during 10 rotation periods was monitored at $TSR = 1.0$, as shown in Figure 8. The calculation procedure accomplishes convergence in the sixth and subsequent rotation periods.

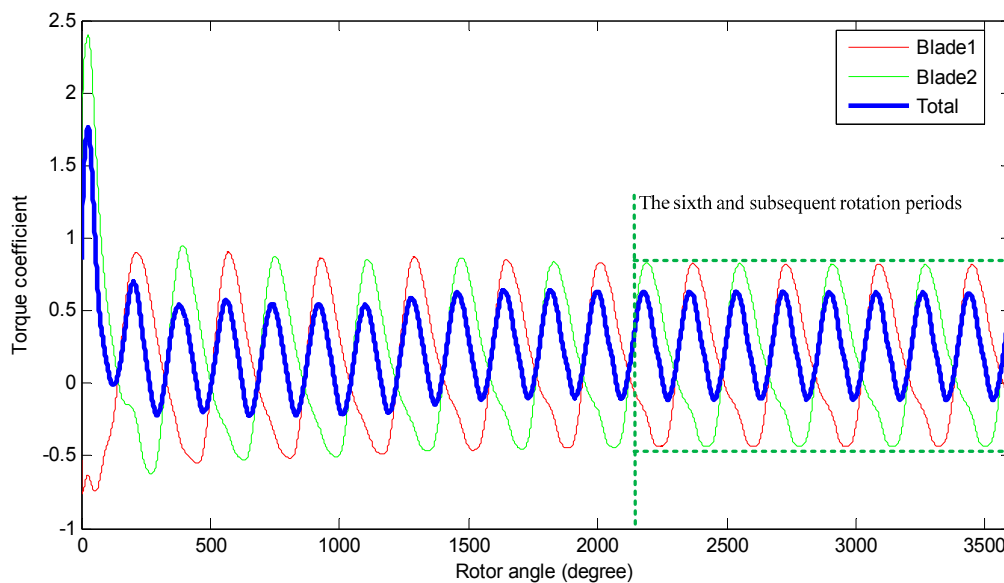


Figure 8. The torque coefficient during 10 rotation periods at $TSR = 1.0$ in the process of computational fluid dynamics (CFD) simulation.

In Figure 9, velocity distribution and pressure distribution were obtained after post-processing, as will be discussed in Section 5.

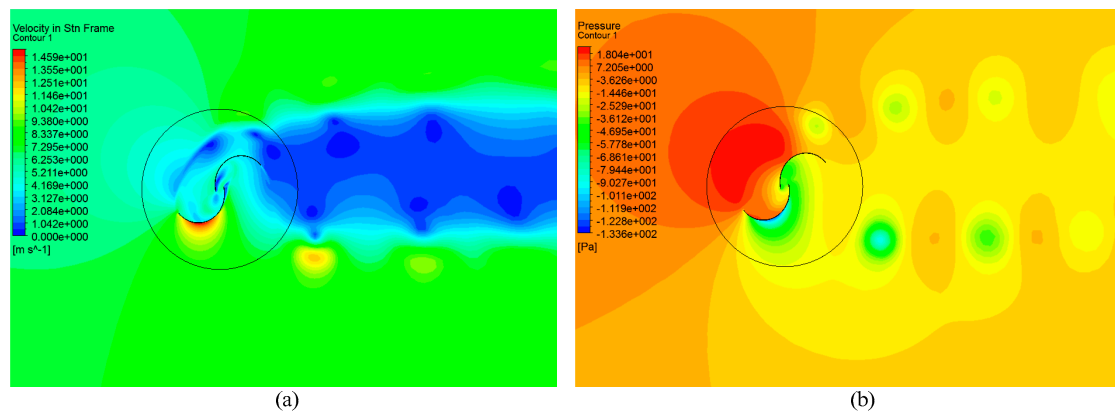


Figure 9. (a) Velocity distribution and (b) pressure distribution around a Savonius turbine.

The instantaneous torque coefficient cyclically varies with the rotor angle, as shown in Figure 10a. Since the two blades are origin-symmetric, instantaneous torque coefficient is cycled twice in a rotation period (0° – 360°) [8]. Averaged power coefficient increase with the *TSR*. The maximum of averaged power coefficient appears at about *TSR* = 1.0. After a fixed value, averaged power coefficient decreases, as shown in Figure 10b.

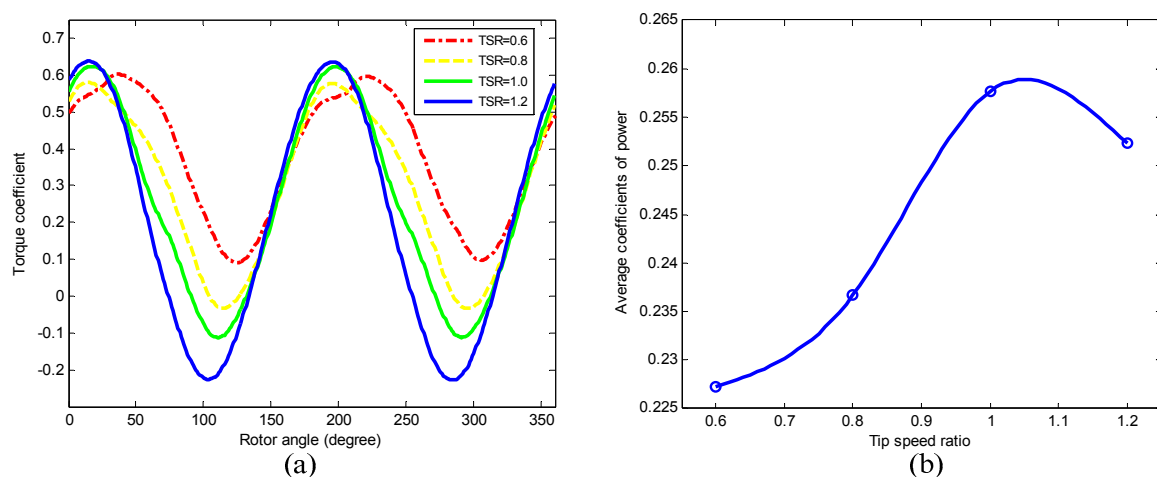


Figure 10. (a) Comparison of the torque coefficient at different rotor angle for the four *TSRs*; and (b) average power coefficient at different *TSRs*.

4. Optimal Design Method

Generally, PSO is a method of searching for the optimal value based on a certain known model (Surrogate model). In this paper, the certain known model is established by using Kriging Method. Kriging Method establishes relation model between optimization objective C_p and design parameters (a_2 and a_1). PSO could find the maximum value of C_p . Finally, the optimal value of C_p corresponds to the optimal design parameters of the blade. There are some similar methods that can be used in this optimization process. When choosing a surrogate model for the optimization problem, Kriging model has been compared with Polynomial response surface model. Obviously, Kriging method is more convenient, faster and more accurate. Meanwhile, PSO has been compared with genetic algorithm (GA). PSO and GA are both global optimization methods. Regarding this optimization question, GA-based iteration takes up to 2–3 times as long as PSO-based iteration. It could be seen that PSO in conjunction with Kriging model is better than similar methods and could satisfy our requirements in practice.

4.1. Kriging Method

Numerous adaptations of design parameters (a_2, a_1) were performed. Generally, Kriging method expresses the unknown function $\hat{y}(X)$ as:

$$\hat{y}(X) = \beta + z(X) \quad (9)$$

where X is an n -dimensional vector (n design variables, a_2 and a_1); β is the linear regression part; and $z(X)$ is the local deviation. $z(X)$ represents a model of a Gaussian and stationary random process with zero mean and covariance:

$$E[z(X)] = 0 \quad (10)$$

$$\text{Var}[z(X)] = \sigma^2 \quad (11)$$

$$E[z(X)z(X_i)] = \sigma^2 R(X, X_i) \quad (12)$$

where σ^2 is the variance of stationary random process; and $R(X, X_i)$ is the spatial correlation function which represents the correlation between $z(X)$ and $z(X_i)$. The spatial correlation function is defined as:

$$R(X, X_i) = \exp\left[-\sum_{k=1}^n \theta_k (X_{ki} - X_k)^2\right] \quad (13)$$

where θ_k is the k th element of correlation vector parameter θ . According to the Spatial Correlation Function, the correlation matrix can be obtained as follows:

$$R = \begin{bmatrix} R(X_1, X_1) & \cdots & R(X_1, X_N) \\ \vdots & \ddots & \vdots \\ R(X_N, X_1) & \cdots & R(X_N, X_N) \end{bmatrix} \quad (14)$$

where $R(X_N, X_N)$ is a spatial correlation function of two known points, and each possible combination of these simple points is described by matrix R . The correlation between an unknown prediction point x and the N known sample points is defined as follows:

$$r(x) = \begin{bmatrix} (R(X, X_1)) \\ \vdots \\ R(X, X_N) \end{bmatrix} \quad (15)$$

The main goal of the paper is to optimize the design of the blade, so the details of the derivations details are not described here. The final Kriging predictor $\hat{y}(X)$ is obtained:

$$\hat{y}(X) = \hat{\beta} + r^T(X)R^{-1}(Y - E(\hat{g}(X))) \quad (16)$$

where $\hat{\beta}$ is the least-squares estimated of β ; and Y is N -dimensional vector:

$$\hat{\beta} = (E^T R^{-1} E)^{-1} E^T R^{-1} Y \quad (17)$$

$$Y = \{y(X_1)y(X_2) \cdots y(X_N)\}^T \quad (18)$$

According to Kriging method, the response surface model has been built as optimization function by using Matlab program.

4.2. Particle Swarm Optimization (PSO)

PSO algorithm simulates the natural swarming behavior of birds flocking. The great ability in global optimal search and avoiding trapping in local optimum are very attractive [20,21,28]. The steps of PSO are as follows:

(1) Initialize N particles (Initial group N design parameters a_2, a_1). The number of random particles is $N = 500$:

$$P1 = (a_{21}, a_{11}), P2 = (a_{22}, a_{12}), P3 = (a_{23}, a_{13}) \dots P500 = (a_{2500}, a_{1500}) \quad (19)$$

(2) Calculate the fitness value (C_p) for each particle according to the certain known model f (Surrogate model):

$$Cp = f(a_2, a_1) \quad (20)$$

where f is derived from Kriging method, and $\hat{y}(X)$ according to Equation (16).

(3) Set the particle P_i with the best fitness value (C_p) in history as personal optimal solution ($pBest$).

(4) Choose the particle P_g with the best fitness value (C_p) of all the particles as the global optimal solution ($gBest$).

(5) Then, for each particle, calculate particle speed according Equations (21) and (22) in the a_2 and a_1 direction.

$$v_{a2} = w \times v_{a2} + c1 \times rand() \times (pBest_{a2} - present_{a2}) + c2 \times rand() \times (gBest_{a2} - present_{a2}) \quad (21)$$

$$v_{a1} = w \times v_{a1} + c1 \times rand() \times (pBest_{a1} - present_{a1}) + c2 \times rand() \times (gBest_{a1} - present_{a1}) \quad (22)$$

where v_{a2} and v_{a1} are particle speed; $pBest_{a2}$ and $pBest_{a1}$ are personal optimal solution; $present_{a2}$ and $present_{a1}$ are present position. $c1$ and $c2$ represent the mean stiffness of the springs pulling a particle. By changing $c1$ and $c2$ one can make the PSO more or less “responsive” and possibly even unstable. The best performance could be obtained by initially setting ω to some relatively high value, which corresponds to a system where particles perform extensive exploration. With an appropriate choice of ω and of the acceleration coefficients ($c1$ and $c2$), the PSO can be made much more stable. In this case, PSO may improve performance. In practice, the values $c1 = c2 = 2.0$, and $\omega = 0.8$ are almost ubiquitously adopted in PSO research [28].

(6) Update particle position according Equations (23) and (24) per unit time t .

$$present_{a2} = present_{a2} + v_{a2} \times t \quad (23)$$

$$present_{a1} = present_{a1} + v_{a1} \times t \quad (24)$$

(7) When the maximum number of iterations or minimum error criteria is attained, the optimization process stops. In this paper, the maximum number of iterations is 200, which is set as the stop criterion. The general procedure of PSO is shown in Figure 11. PSO is implemented in a computer program (using Matlab language) in conjunction with Kriging model. The procedure outputs are optimal value C_p . Then, two variables representing design parameters (a_2 and a_1) of the turbine are translated from Kriging model. Hence, with the help of PSO, the optimal design parameters can be found.

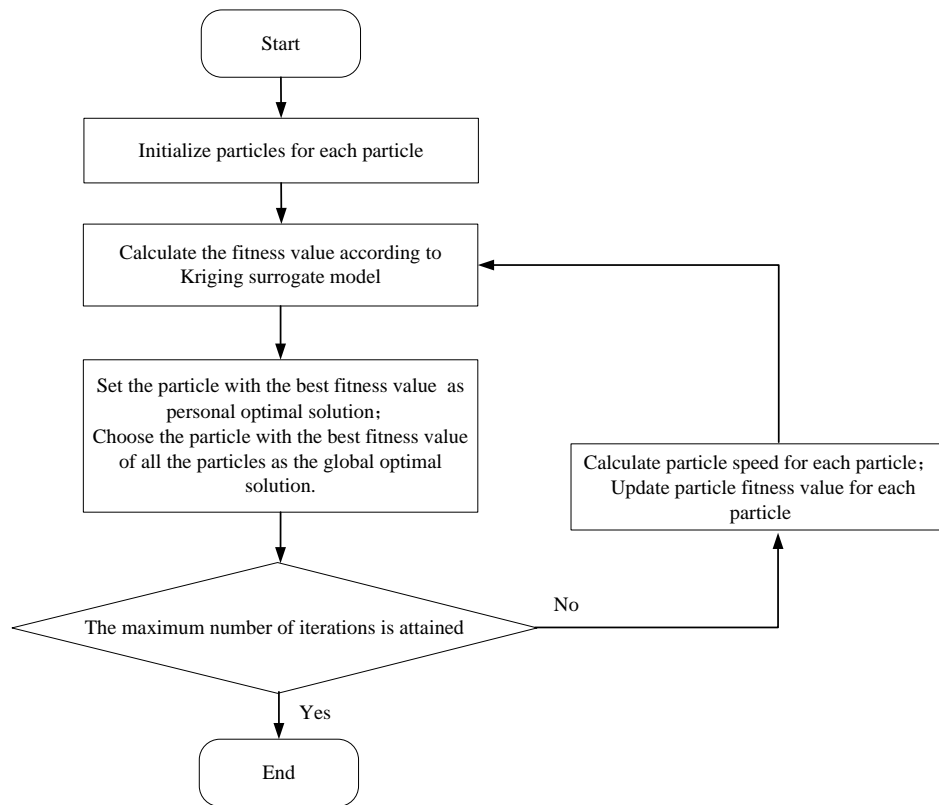


Figure 11. The general procedure of particle swarm optimization (PSO).

4.3. Optimization Results

The optimization procedure is divided into two steps: Firstly, a global Kriging response surface model was established in feasible region (Figure 3), as shown in Figure 12a. In this step, 36 Savonius turbines were investigated. The optimal range of design parameters converged at a local region were determined, as shown in Figure 12b. Global response surface model is generally rough estimate, but it will narrow down the region of a_2 and a_1 , which has contributed to establish a more precise response surface model.

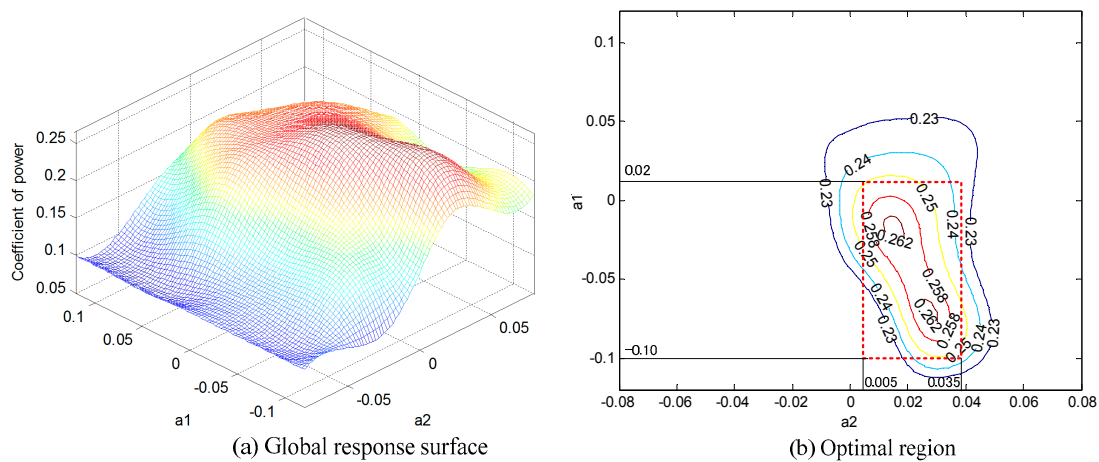


Figure 12. Global response surface and optimal region.

Secondly, 25 Savonius turbines were added as sample points in the local optimal region. Hence, a more precise Kriging response surface model was established, as shown in Figure 13a. Through the

iterative search in local optimal region, the optimal point was directly obtained using PSO. The optimal point is marked in Figure 13b. The coordinate values of the optimal point represent the design parameters ($a_2 = 0.017902$ and $a_1 = 0.039233$) of the optimal blade.

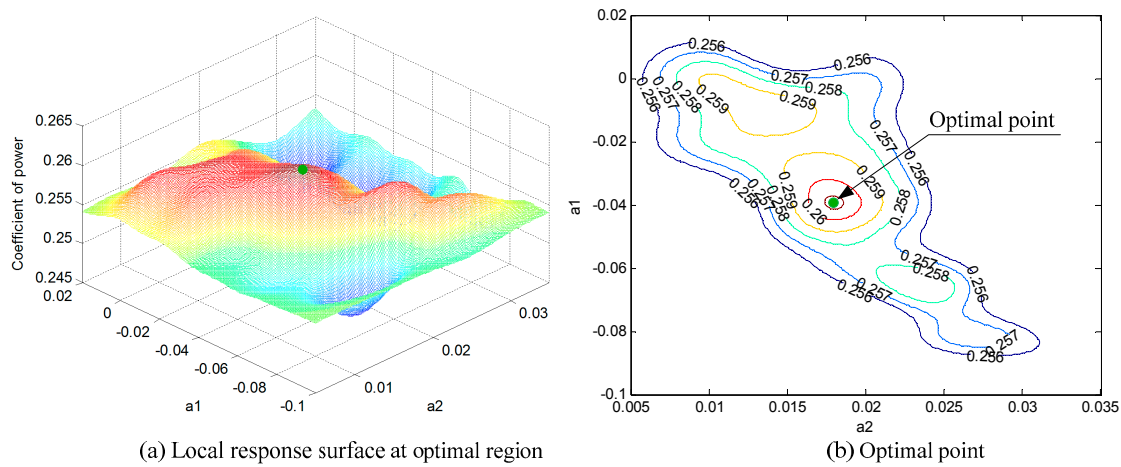


Figure 13. Local response surface and optimal point.

Finally, an optimal design, which satisfies all restrictions and makes C_p of the Savonius turbine reach maximum value, was obtained. The characteristic of the optimal Savonius turbine will be investigated in the following sections.

5. Results and Discussion

5.1. Comparison of the Geometries

After a series of optimization process, we obtained the optimal design parameters for the modified Savonius, when its C_p achieves maximum value (significantly enhanced from 0.247 to 0.262). The shape of the optimal Savonius blade and the classical Savonius blade is compared in Figure 14. The profile shape of optimal blade looks like a “hook”. There are similar conclusions from previous studies using other design methods [16,24]. The profile of the blade close to the central axis becomes narrower, while the profile of blade far from the central axis becomes wider.

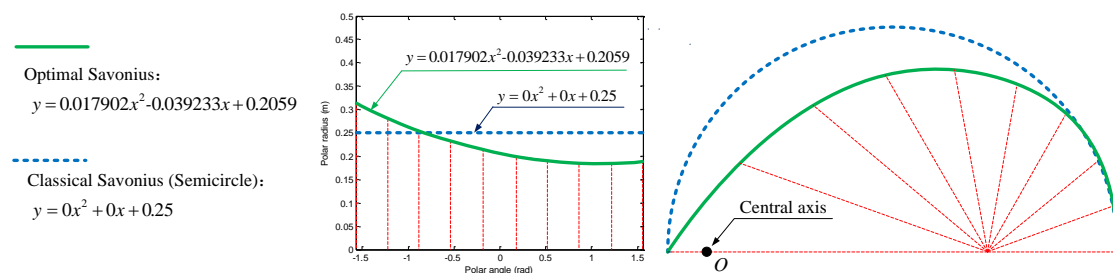


Figure 14. Comparison of the shape for the Classical Savonius and the Optimal Savonius.

Due to the new profile shape of the optimal blade, there are many obvious improvements. Firstly, when the blade work as an advancing blade (Figure 15), the optimal blade will hold more air at a greater distance $L1$. Airflow will be directed more to the distal of the blade. By contrast, the classical blade just holds air in its center, which is the source of lower efficiency of classical Savonius. The arm of air force of the optimal blade $L1$ is obviously greater than that of the classical blade $L2$. Therefore, the optimal blade will obtain more driving torque and power from air than the classical blade. Secondly, the optimal blade with a smaller size has the advantageous to decrease the drag during the returning

process and cut costs. The air pressure acting on the optimal blade is higher than the classical blade in most cases, as shown in Figure 19. Finally, by comparing the torque coefficient C_m and the power coefficient C_p in the whole rotation process for the classical Savonius and the optimal Savonius, C_m and C_p become greater after optimization in most cases, as shown in Figures 20–22. More details will be discussed in the following sections.

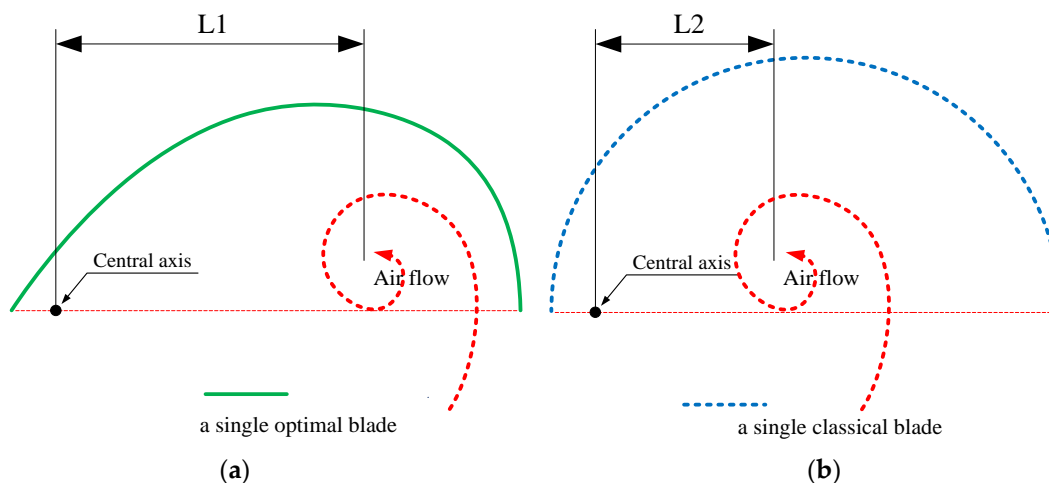


Figure 15. Simplified air flow diagram acting on the classical Savonius and the optimal Savonius.

Compared with other similar studies, only two design parameters are used for the shape-complicated blade. The adoption of the two parameter approach simplifies the difficulty and complexity of the design of blades. Therefore, the optimal design is suitable for mass production. In addition, the optimal results provide a new design idea and reference resources for further investigations. Cubic polynomial curve or higher order curve could be used to describe a more precise blade in the future. However, for now, the bent second order polynomial is acceptable as an optimal design, since the Savonius wind turbine obtained its highest power coefficient C_p by using minimal parameters (only two design parameters). Main geometric parameters are listed in Table 4. Moreover, according to relative weight, the weight of the optimal blade is significantly reduced by 17.9%.

Table 4. Comparison of geometric parameters of a blade.

Type of the Designs	Design Parameters	Height h (m)	Relative Weight
Initial design (Classical)	$R = 0.25$	0.25	1
Optimal design	$a_2 = 0.017902$ $a_1 = 0.039233$	0.206	0.821

5.2. Flow Structure

There is a great wake of the turbine about 7D in the downstream. The flow structure of the wake is similar to the structure of a Karman vortex street [25], as shown in Figure 16a. According to the velocity distribution, a large number of rotating vortices are visible. The intensity of these vortices decreases with time. In the position of rotating vortices, low-pressure areas appear correspondingly, as shown in Figure 15b. For the optimal blade, the distance between the center of pressure and the central axis is obviously greater than that of the classical blade. Thus, the arm of the resultant of the forces of the optimal blade is obviously greater than that of the classical blade. Therefore, the optimal blade would obtain more driving torque and power from air than the classical blade.

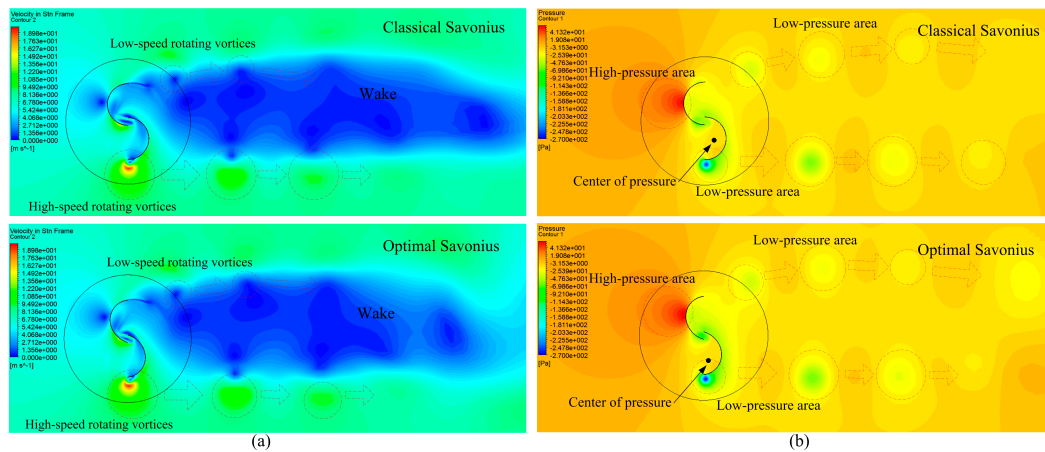


Figure 16. (a) Velocity distribution and (b) pressure distribution around the classical Savonius and optimal Savonius.

Velocity distributions around the optimal Savonius turbine at different rotor angles are shown in Figure 17. Because the turbine is origin-symmetric, the velocity distributions at the rotor angle of 0° , 45° , 90° , and 135° can be used to describe flow characteristics in a whole rotation period. Rotating blade wake appears indistinctly following the returning blade, as shown in Figure 17a,b. Stagnation point appears on the convex side of the returning blade, as shown in Figure 17c,d. High-speed rotating vortices gradually separate from the advancing blade at about 135° , as shown in Figure 17d. The overlap ratio and the spacing have a significant impact on the performance of the Savonius turbines [4,29]. The optimization objective is the shape of blade in this paper, so other design variables (for instance, overlap ratio) are not analyzed in detail.

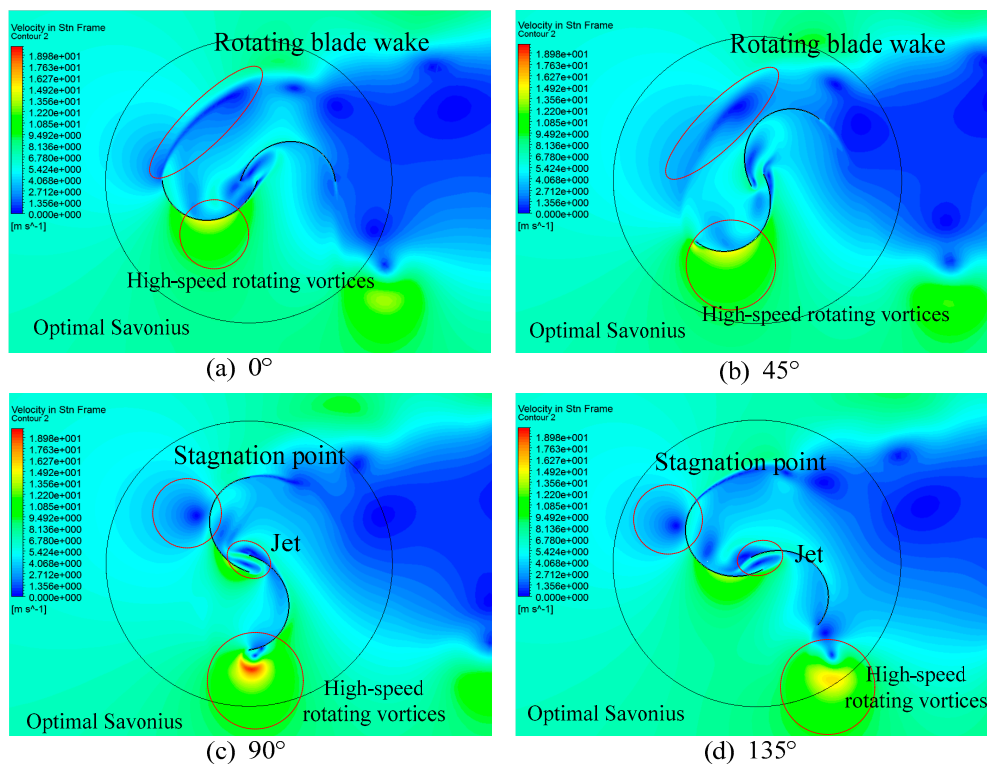


Figure 17. Velocity distributions of the local flow at different rotors angular positions for the optimal Savonius.

5.3. Pressure Distributions

Pressure distributions of the flow field around the turbine are presented. At the rotor angle of 0° (Figure 18a), a high-pressure area can be observed at the concave side of the advancing blade, and a low-pressure area can be observed at the convex side of the advancing blade. At 45° (Figure 18b), pressure distributions around the advancing blade are similar to 0° rotor angle. A high-pressure area acts on the convex side of the returning blade, and a low pressure area acts on the concave side. The pressure differential provides a great torque inhibiting the rotation of the turbine rotor. At 90° (Figure 18c), a great low-pressure area appears at the top of the advancing blade. The pressure differential of the returning blade has a moment arm which creates negative torque inhibiting the rotation of the rotor. At 135° (Figure 18d), this great low-pressure area leaves the top of advancing blade. The distance between the center of pressure and the central axis is obviously greater after optimization.

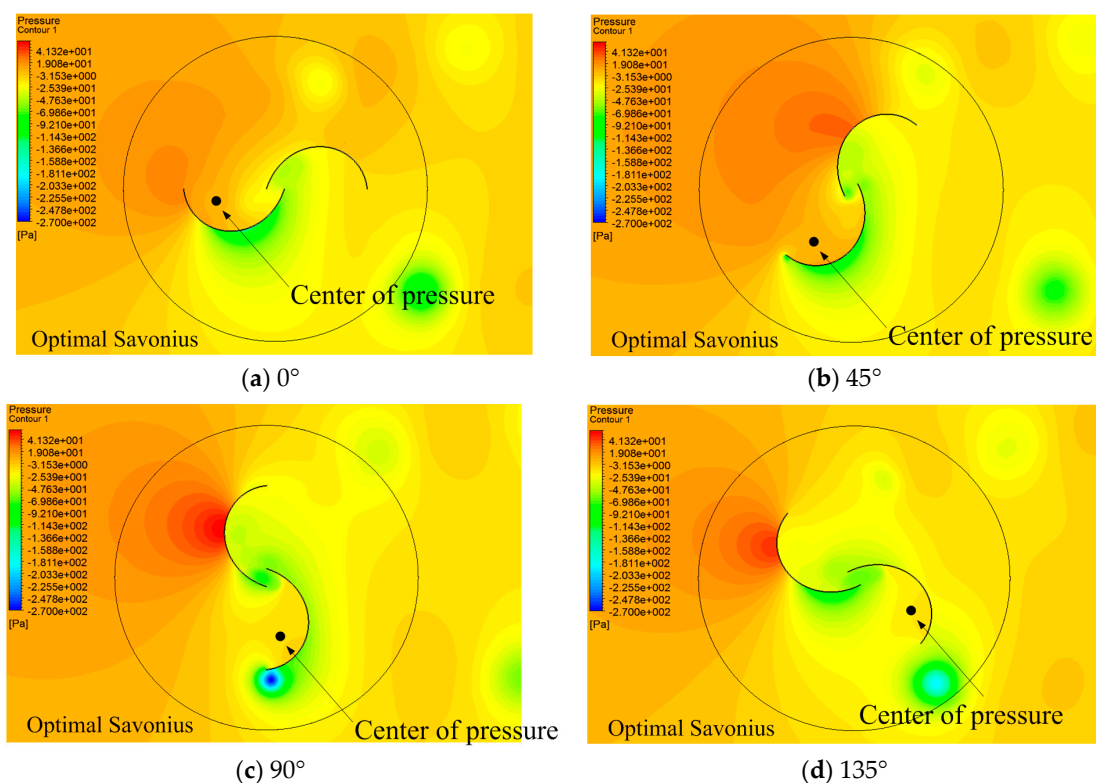


Figure 18. Pressure distributions of the local flow at different rotors angular positions.

In practice, to maintain the stable power network frequency to ensure the quality of power supply, the rotary speed of wind turbine or generator is limited to a fixed value ω . Therefore, the $TSR = \omega D / (2v)$ is a fixed value under specific wind speed v . Figure 19a–h shows dynamic simulations at different times (at different rotation angles) under specific rotary speed ω of wind turbine.

Comparison of pressure distributions on the blade will give a precise explanation of that where the improvements of the optimal blade's performance occur. The pressure distribution on a single blade at 0° , 45° , 90° , 135° , 180° , 225° , 270° and 315° are compared, as shown in Figure 19a–h. Pressure distributions on the concave side of the Classical Savonius (C-CS), the convex side of the Classical Savonius (V-CS), the concave side of the Optimal Savonius (C-OS) and the convex side of the Optimal Savonius (V-OS) are drawn in Figure 18. Pressure differential between inside and outside of the Classical Savonius (PD-CS) and the Optimal Savonius (PD-OS) are also drawn. By analyzing pressure differential, the curve of PD-OS (Green Line) is located upper side of the curve of PD-CS (Green Dotted Line) in most cases. The Optimal Savonius blade is obviously superior to the classical design.

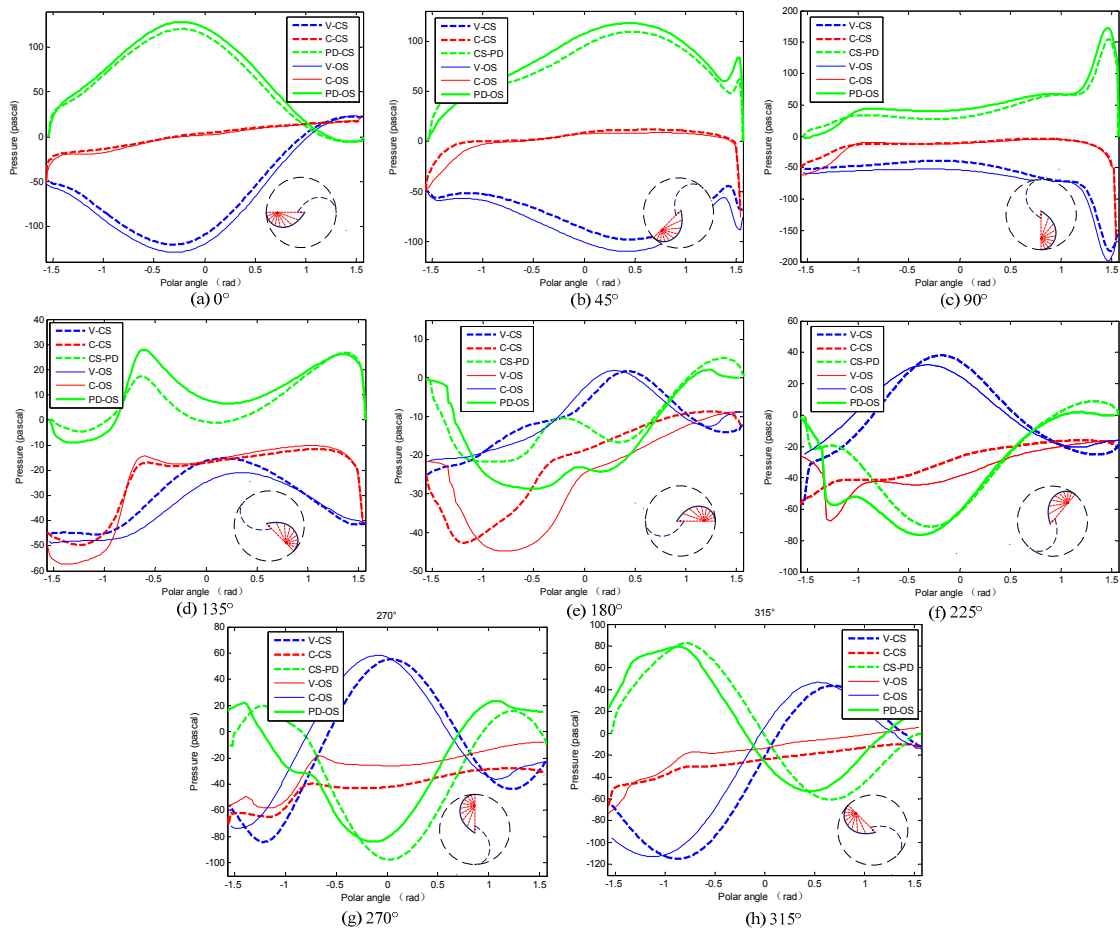


Figure 19. Pressure distributions of a single blade at different rotors angular positions.

5.4. Torque and Power Analysis

The variation of the instantaneous torque coefficient with the rotor angle at different TSR is shown in Figure 20. The amplitude of instantaneous C_m increases with the TSR . They have a similar change rule, but the optimal design is obviously higher than classical design.

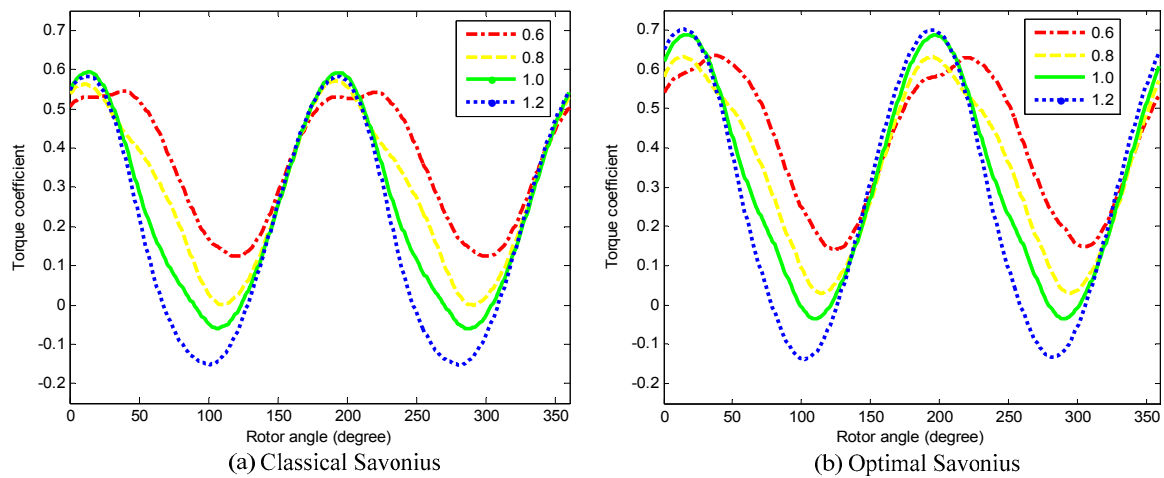


Figure 20. (a) Classical Savonius and (b) optimal Savonius: comparison of the torque coefficient for the four $TSRs$.

By comparing instantaneous C_m for the classical Savonius and optimal Savonius at the same TSR ($TSR = 1.0$), the amplitude of C_m becomes greater after optimization. The instantaneous C_m is optimized as shown in Figure 21.

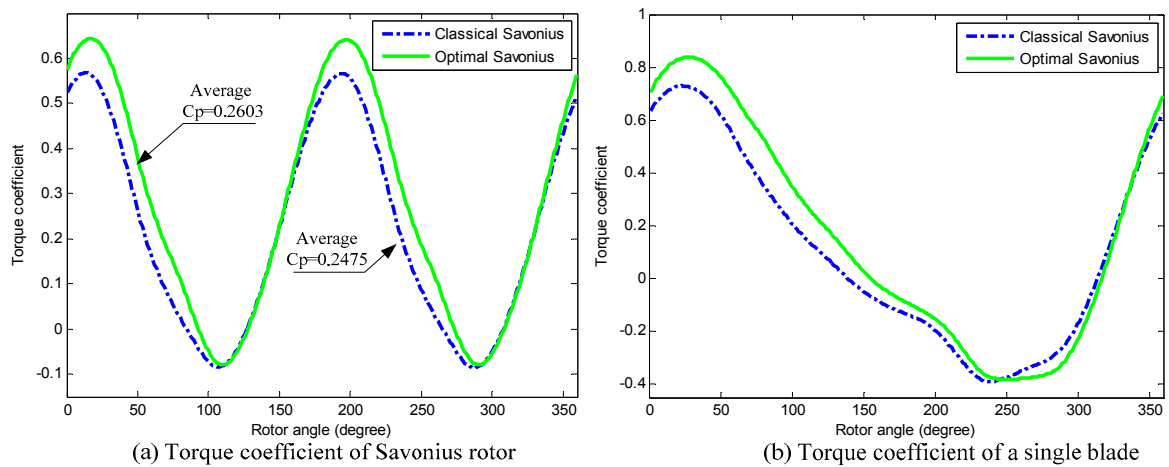


Figure 21. (a) Savonius rotor and (b) a single blade: comparison of the instantaneous C_p .

While investigating the variation of the average C_m and C_p with $TSRs$, the optimal Savonius turbine exhibits superior characteristics. Figure 22a presents a comparison of averaged C_m . Figure 22b presents a comparison of averaged C_p . The values of averaged C_p increase with TSR . The classical Savonius and the optimal Savonius attain their peak performance at a similar TSR . After a certain value (at about $TSR = 1.0$), averaged power coefficients decrease.

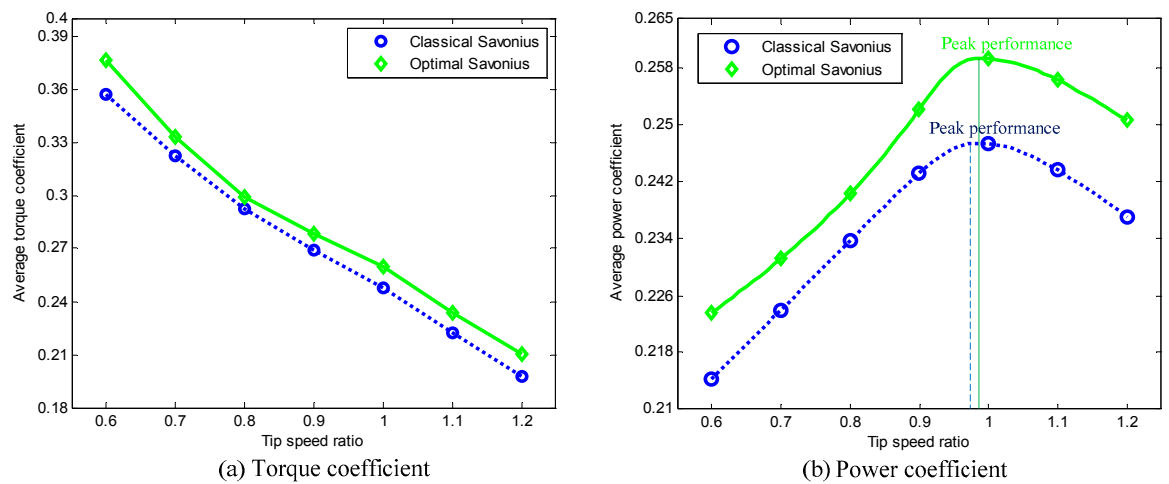


Figure 22. Comparison of (a) average C_m and (b) average C_p at different $TSRs$ for the classical Savonius and the optimal Savonius.

Main performance parameters are listed in Table 5 at peak performance. The optimization objective C_p is significantly increased. The results illustrate the effectiveness and validity of the optimal design method.

Table 5. Comparison of main performance parameters.

Optimization Objective	Initial Design (Classical)	Optimal Design	Optimization Effect
C_p	0.2477	0.2623	+6%

6. Conclusions

To obtain the highest power output, a novel parametric modeling and optimization method for Savonius wind turbines was proposed by referring to polar coordinates. Only two design parameters were set to describe a blade, which is a great improvement for the optimization process. Sixty-one geometries of Savonius wind blades were numerically analyzed using CFD method. Numerical simulation results were compared to the experimental data, which verified the feasibility of the numerical method. Response surface surrogate models were established according to Kriging method. Accordingly, PSO algorithm was presented to obtain the optimal design parameters of the Savonius blade. By comparing the optimal Savonius turbine with the classical design, the main outcomes could be outlined below:

- (1) A shape-complicated blade described by a bent quadratic polynomial curve is obtained. The shape of the optimal Savonius blade looks like a “hook”, with design parameters $a_2 = 0.017902$ and $a_1 = 0.039233$. To describe a more precise blade, cubic polynomial curve or higher order curve could be used in the future.
- (2) In terms of the average C_p , the optimal Savonius turbine is superior to the classical design. Optimization objective C_p is significantly increased from 0.247 to 0.262. Moreover, the weight of the optimal blade is reduced by 17.9%.
- (3) The amplitude of instantaneous C_m of the optimal Savonius is obviously higher than that of the classical Savonius.
- (4) Comprehensive performances of the optimal Savonius had gained high improvements during the entire period after optimization. However, wind turbine performance is not improved significantly in the returning process. This enlightens us that reducing wind torque during the returning process is a future trend.

This study intended to propose a new parametric design ideology to describe and optimize the Savonius wind turbine blade using the minimal design parameters. Depending on this optimal design of the Savonius blade, other design variables could be considered to further increase efficiency.

Acknowledgments: This research was supported by the National Science Foundation of China (Grant No. 61572404) and the Science and Technology Nova Plan of Shaanxi Province (Grant No. 2016KJXX-57).

Author Contributions: Baoshou Zhang and Baowei Song designed the study and performed the simulations. Zhaoyong Mao and Wenlong Tian analyzed the data and wrote the paper. Boyang Li and Bo Li reviewed and edited the manuscript. All authors read and approved the manuscript.

Conflicts of Interest: The authors declare no conflict of interest.

References

1. Wang, Y.F.; Zhan, M.S. 3-Dimensional CFD simulation and analysis on performance of a micro-wind turbine resembling lotus in shape. *Energy Build.* **2013**, *65*, 66–74. [[CrossRef](#)]
2. Tian, W.; Song, B.; Vanzwieten, J.; Pyakurel, P. Computational fluid dynamics prediction of a modified Savonius wind turbine with novel blade shapes. *Energies* **2015**, *8*, 7915–7929. [[CrossRef](#)]
3. Zhao, Z.; Zheng, Y.; Xu, X.; Liu, W.; Hu, G. Research on the improvement of the performance of Savonius rotor based on numerical study. In Proceedings of the IEEE International Conference on Sustainable Power Generation and Supply (SUPERGEN'09), Nanjing, China, 6–7 April 2009; pp. 1–6.
4. Akwa, J.V.; Vielmo, H.A.; Petry, A.P. A review on the performance of Savonius wind turbines. *Renew. Sustain. Energy Rev.* **2012**, *16*, 3054–3064. [[CrossRef](#)]
5. Altan, B.D.; Atilgan, M. An experimental and numerical study on the improvement of the performance of Savonius wind rotor. *Energy Convers. Manag.* **2008**, *49*, 3425–3432. [[CrossRef](#)]
6. Wahyudi, B.; Soeparman, S.; Hoeijmakers, H.W.M. Optimization design of Savonius diffuser blade with moving deflector for hydrokinetic cross flow turbine rotor. *Energy Procedia* **2015**, *68*, 244–253. [[CrossRef](#)]

7. Kumar, D.; Sarkar, S. Numerical investigation of hydraulic load and stress induced in Savonius hydrokinetic turbine with the effects of augmentation techniques through fluid-structure interaction analysis. *Energy* **2016**, *116*, 609–618. [[CrossRef](#)]
8. Kacprzak, K.; Liskiewicz, G.; Sobczak, K. Numerical investigation of conventional and modified Savonius wind turbines. *Renew. Energy* **2013**, *60*, 578–585. [[CrossRef](#)]
9. Alaimo, A.; Esposito, A.; Milazzo, A.; Orlando, C.; Trentacosti, F. Slotted blades Savonius wind turbine analysis by CFD. *Energies* **2013**, *6*, 6335–6351. [[CrossRef](#)]
10. Altan, B.D.; Atılgan, M. A study on increasing the performance of Savonius wind rotors. *J. Mech. Sci. Technol.* **2012**, *26*, 1493–1499. [[CrossRef](#)]
11. El-Askary, W.A.; Nasef, M.H.; Abdel-Hamid, A.A.; Gad, H.E. Harvesting wind energy for improving performance of Savonius rotor. *J. Wind Eng. Ind. Aerodyn.* **2015**, *139*, 8–15. [[CrossRef](#)]
12. Modi, V.J.; Roth, N.J.; Fernando, M.S.U.K. Optimum-configuration studies and prototype design of a wind-energy-operated irrigation system. *J. Wind Eng. Ind. Aerodyn.* **1984**, *16*, 85–96. [[CrossRef](#)]
13. Zhou, T.; Rempfer, D. Numerical study of detailed flow field and performance of Savonius wind turbines. *Renew. Energy* **2013**, *51*, 373–381. [[CrossRef](#)]
14. Mohamed, M.H.; Janiga, G.; Pap, E.; Thévenin, D. Optimal blade shape of a modified Savonius turbine using an obstacle shielding the returning blade. *Energy Convers. Manag.* **2011**, *52*, 236–242. [[CrossRef](#)]
15. Driss, Z.; Mlayeh, O.; Driss, D.; Maaloul, M.; Abid, M.S. Numerical simulation and experimental validation of the turbulent flow around a small incurved Savonius wind rotor. *Energy* **2014**, *74*, 506–517. [[CrossRef](#)]
16. Ahmed, M.R.; Faizal, M.; Lee, Y.H. Optimization of blade curvature and inter-rotor spacing of Savonius rotors for maximum wave energy extraction. *Ocean Eng.* **2013**, *65*, 32–38. [[CrossRef](#)]
17. Al Faruk, A.; Sharifian, A. Geometrical optimization of a swirling Savonius wind turbine using an open jet wind tunnel. *Alex. Eng. J.* **2016**, *55*, 2055–2064. [[CrossRef](#)]
18. Dragomirescu, A. Performance assessment of a small wind turbine with crossflow runner by numerical simulations. *Renew. Energy* **2011**, *36*, 957–965. [[CrossRef](#)]
19. Martin, J.D.; Simpson, T.W. Use of Kriging models to approximate deterministic computer models. *AIAA J.* **2005**, *43*, 853–863. [[CrossRef](#)]
20. Kennedy, J. The particle swarm: Social adaptation of knowledge. In Proceedings of the IEEE International Conference on Evolutionary Computation, Indianapolis, IN, USA, 13–16 April 1997; pp. 303–308.
21. Eberhart, R.C.; Kennedy, J. A new optimizer using particle swarm theory. In Proceedings of the 6th International Symposium on Micro Machine and Human Science, Nagoya, Japan, 4–6 October 1995; Volume 1, pp. 39–43.
22. Juang, C.F. A hybrid of genetic algorithm and particle swarm optimization for recurrent network design. *IEEE Trans. Syst. Man Cybern. Part B Cybern.* **2004**, *34*, 997–1006. [[CrossRef](#)]
23. Sheldahl, R.E.; Feltz, L.V.; Blackwell, B.F. Wind tunnel performance data for two-and three-bucket Savonius rotors. *J. Energy* **1978**, *2*, 160–164. [[CrossRef](#)]
24. Saha, U.K.; Thotla, S.; Maity, D. Optimum design configuration of Savonius rotor through wind tunnel experiments. *J. Wind Eng. Ind. Aerodyn.* **2008**, *96*, 1359–1375. [[CrossRef](#)]
25. Menet, J.L. A double-step Savonius rotor for local production of electricity: A design study. *Renew. Energy* **2004**, *29*, 1843–1862. [[CrossRef](#)]
26. Wenlong, T.; Baowei, S.; Zhaoyong, M. Conceptual design and numerical simulations of a vertical axis water turbine used for underwater mooring platforms. *Int. J. Naval Arch. Ocean Eng.* **2013**, *5*, 625–634. [[CrossRef](#)]
27. McTavish, S.; Feszty, D.; Sankar, T. Steady and rotating computational fluid dynamics simulations of a novel vertical axis wind turbine for small-scale power generation. *Renew. Energy* **2012**, *41*, 171–179. [[CrossRef](#)]
28. Chen, H.N.; Zhu, Y.L.; Hu, K.Y.; Ku, T. Global optimization based on hierarchical coevolution model. In Proceedings of the IEEE Congress on Evolutionary Computation (CEC 2008), Hong Kong, China, 1–6 June 2008; pp. 1497–1504.
29. Bhutta, M.M.A.; Hayat, N.; Farooq, A.U.; Ali, Z.; Jamil, S.R.; Hussain, Z. Vertical axis wind turbine—A review of various configurations and design techniques. *Renew. Sustain. Energy Rev.* **2012**, *16*, 1926–1939. [[CrossRef](#)]

